Investigation of the strength and trend of seismic anisotropy beneath the Zagros collision zone

Seyed-Jasser Motavalli-Anbaran[1], Ali Moradi[2*], and Ayoub Kaviani[3]

[1]*M. Sc., Institute of Geophysics, University of Tehran, Tehran, Iran*
[2]*Assistant Professor, Institute of Geophysics, University of Tehran, Tehran, Iran*
[3]*Research Associate, Institute of Geosciences, Goethe University Frankfurt, Frankfurt, Germany*

(Received: 27 February 2018, Accepted: 27 June 2018)

Abstract

The Zagros collision zone is known as an active tectonic zone that represents the tectonic boundary between the Eurasian and Arabian plates. A popular strategy for gaining insight into the upper mantle processes is to examine the splitting of seismic shear waves and interpret them in terms of upper mantle anisotropy and deformation. Core phases SK(K)S from over 278 earthquakes ($M_W \geq 6.0$) occurred between years 2010 and 2017 at epicentral distances between 90° and 145° are examined, which were recorded by 27 broadband stations located in the Zagros collision zone. In compressional tectonic regimes such as the Zagros collision zone, a dominant pure shear deformation in the mantle is expected that could develop lattice preferred orientation (thus anisotropic fabrics) subparallel to the strike of the mountain belt. The findings show that the majority of the fast axes of seismic anisotropy are oriented in the NE-SW direction (perpendicular to the trend of the belt) with delay times (a proxy for the strength of anisotropy) varying between 1 and 1.5 seconds. If deformation in the mantle lithosphere was the main factor of the observed anisotropy, then the fast direction of anisotropy would be parallel to the belt. Therefore, the main source of anisotropy is thought to be residing in the sub-lithosphere mantle. Crack-induced anisotropy in the upper crust that can be perpendicular to the trend of the belt (parallel to the maximum compressional stress direction) may also have some contribution to the observed splitting of shear-waves.

Keywords: seismic anisotropy, shear-wave splitting, SKS splitting, Zagros

*Corresponding author: asmoradi@ut.ac.ir

1 Introduction

Current active tectonics in the Iranian plateau is the result of the convergence between the Arabian plate in the southwest and Eurasian plate in the northeast (Jackson and McKenzie, 1984) at a rate of about 22 mm per year (Sella et al., 2002). This continent-continent collision zone has a highly complex structure that has been developed by various geodynamic mechanisms by which the still active tectonics of the area is being driven (e.g. Dewey et al., 1986; Barazangi et al., 2006). The Zagros Mountain belt constitutes one of the youngest and most active orogenic belts on the Earth (Snyder and Barazangi, 1986), which were formed as a consequence of the collision between the aforementioned plates. An orogenic belt develops when a continental plate crumples and is pushed upwards to form mountain ranges; the Orogeny is therefore the primary mechanism by which mountains are built on continents (Kearey et al., 2013; Waltham, 2014). The Zagros collision system is composed of three major tectonically parallel units with an NW–SE trend: (1) Zagros fold-thrust belt (ZFTB), (2) the Sanandaj-Sirjan metamorphic zone which overthrusts the ZFTB along the Main Zagros Thrust, and (3) Urumieh–Dokhtar Magmatic Arc (Alavi, 1994). The ZFTB consists of sedimentary rocks of different geological periods in the northern margin of the Arabian plate and southwest of the Iranian plateau (Sepehr and Casgrov, 2005) on the Precambrian metamorphic scope (Berberian, 1995). Due to the existing compressional regime in the region, and also the unique situation of the Iranian plateau in terms of its surrounding plates, the Zagros has undergone several episodes of deformation as well as other geodynamical processes. The knowledge of such tectonic interactions is necessary to identify the tectonic history of the Zagros. The study of seismic anisotropy can help address such tectonic processes as well as large scale patterns of sub-lithospheric mantle flows [e.g., Vinnik et al., 1989, 1992; Fouch et al., 2000; Sleep et al., 2002], and the preferential orientation of fluid or melt bodies [e.g., Sleep, 1997]. Seismic anisotropy is the dependence of seismic wave velocities to the propagation and polarization directions of the wave. The results of recent mineral physics indicate that stress, temperature, and pressure conditions, together with volatile content can affect anisotropic fabric (e.g., Jung and Karato, 2001; Mainprice, 2007; Karato et al., 2008; Jung et al., 2009). In the upper mantle, the deformation of an aggregate of mantle mineral crystals in the presence of high strain causes anisotropy by developing a Lattice Preferred Orientation (LPO). Since the olivine is the main mineral in upper mantle (Stein and Wysession, 2009), LPO in olivine is one of the best possible candidates for upper mantle anisotropy. Because of causal connection anisotropy and lithosphere and asthenosphere deformation, its study is now one of the classical issues in seismology, and the interpretation of seismic anisotropy has become a vital tool in the study of dynamic processes within the Earth's mantle (Long and Silver, 2009). Using SKS splitting analysis of data from 14 permanent and more temporary broadband stations, Kaviani et al. (2009) reported mainly null splitting measurements in the Zagros. However, Keshvari et al. (2011), using variations in the relative S-residuals, observed an apparent effect resulting from anisotropy beneath a profile across the Zagros. In this study, it is tried to study the seismic anisotropy beneath the Zagros using better station and data coverage.

2 Methodology

Shear waves split into two independent and perpendicularly polarized waveforms when entering an anisotropic media. These two wave fields travel along very close paths but with different speed. The orientations of the fast and slow shear waves are related to the principal axes of anisotropy. The resultant shear wave splitting (SWS) can be described by the polarization direction of the faster shear wave arrival, φ, and the time lag, δt, between these two shear waves. Core phases such as SKS are radially polarized when emerges from the core–mantle boundary (CMB). Due to the S–P and P–S conversions at the CMB, any observed splitting can be attributed to the receiver side ray path. There are various methods to characterize the seismic anisotropy using core phases, which is often developed by measuring the SWS parameters from broadband data. These methods comprise of several processing steps such as: 1) filtering, 2) rotation of seismogram components, 3) selection of records with high signal-to-noise ratio (SNR), 4) choosing a time window for the analysis, 5) visual inspection or statistical analysis of results, and 6) error estimates (Long and Silver, 2009).

In this study, the approach developed by Silver and Chan (1991) is followed in which by applying the rotation to both horizontal components and then applying time delay on one component, a corrected radial and transverse component is created. By plotting the energy contour map of the corrected transverse component of core phases, e.g. SKKS, SKS, an optimal amount of the shear-wave splitting parameters (φ, δt) and estimation errors can be obtained (Silver and Chan, 1991; Savage, 1999). This method is the most commonly used splitting measurement known as transverse component minimization method (TM). This method applies to the horizontal components, rotated into a radial (R) and transverse (T) coordinate system, where the so-called radial component corresponds to the back azimuthal direction for core phases (Sileny and Plomerova, 1996; Vecsey et al., 2008). The transverse component minimization method is based upon the fact that in the absence of anisotropy, a shear wave is linearly polarized and no delay occurs between the horizontal components. The method performs a grid search over all possible values of φ and δt, then it rotates and time-shifts the horizontal components appropriately and measures the amount of energy on the corrected transverse component. Finally, it produces a contour plot of transverse component energy for all possible pairs of splitting parameters. The best-fitting parameters correspond to the minimum energy on this contour plot and formal errors on the measurements are estimated using an F-test formulation (Silver and Chan, 1991). This test is performed for each set of possible φ and δt to determine whether or not these parameters are within the bounds of a 95 percent confidence region.

3 Data and processing

In this study, a data set from 27 broadband seismic stations (Table 1) of the Iranian Seismological Center, IRSC, operated by the Institute of Geophysics, University of Tehran (IGUT) is used. The NEIC catalogue is searched to identify suitable events ($M_W \geq 6.0$) between 2011 and 2017 occurred in the distance range 90 to 145 . Waveforms of 280 earthquakes have been used in this study. Data was recorded by various type of seismic sensors, Trillium 40 sec (16 stations), Trillium 120 sec (11 stations) and CMG3T (2 stations). The Trillium sensors were connected to Taurus Digitizers and CMG3T was connected to CMG24DM Digitizers. All stations were recording data with 50 sps.

Table 1. The information of IRSC broadband stations is used in present research.

No.	Code	Latitude (°)	Longitude (°)	Elevation (M)	Place	Start time yyyy|m|d			Natural period (S)
1	MAHB	36.7666	45.71	1370	Mahabad	2013	3	10	120
2	DHR	34.6997	46.3867	1840	Dehrash	2013	3	1	120
3	LIN	34.9187	46.9625	2140	Layen	2013	3	1	120
4	BZA	34.4696	47.8605	2330	Bozab	2012	5	1	120
5	KOM	34.1761	47.5144	1716	Komasi	2012	5	14	40
6	KCHF	34.2750	47.0404	1715	Cheshme Sefid	2013	4	1	40
7	KFM	33.5244	47.8469	1676	KafarMosalman	2012	2	1	120
8	KMR	33.5178	48.3803	1733	Kamar Siah	2012	5	1	120
9	HAGD	34.8220	49.1390	1831	Aqdareh	2011	4	1	40
10	HKZM	35.3775	48.9045	2328	Kuhzaman	2011	4	1	40
11	HSAM	34.2116	48.6023	2314	Samen	2011	4	1	40
12	KLNJ	31.0084	51.5921	2660	Kalanja	2012	10	1	40
13	AHWZ	31.3298	48.6437	19	Ahwaz	2013	2	1	360
14	AMIS	31.6652	49.2866	442	Masjed Soleyman	2015	1	6	120
15	ABH1	30.5999	50.2531	346	Behbahan	2015	1	7	120
16	SHK1	32.3280	50.8845	2093	Shahrekord	2014	12	1	40
17	SHI	29.6374	52.5201	1600	Shiraz	2010	1	1	40
18	LMD1	27.3398	53.1646	425	Lamerd	2013	5	19	40
19	LAR1	27.6694	54.3746	785	Laar	2013	12	23	120
20	JHRM	28.5050	53.5770	998	Jahrom	2011	10	1	40
21	DHL1	32.6810	47.2807	204	Dehloran	2014	8	19	40
22	BNB	27.4490	56.5400	62	Bandar Abbas	2008	2	1	360
23	GENO	27.3998	56.1721	1616	Geno	2010	05	1	40
24	JSK1	25.6379	57.7701	15	Jask	2013	5	15	120
25	KHNJ	27.9477	57.7056	492	Kahnooj	2013	05	15	120
26	ROKH	32.3992	51.0722	2022	Rokhbas	2011	04	30	40
27	JHBN	32.2312	50.6657	2657	Jahanbin	2011	05	02	40

After the earthquake database was prepared, all waveforms were band-pass filtered to retain energy between 0.05 to 0.2 Hz. The arrival of the SK(K)S phases are identified by calculating the theoretical arrival times of these phases using the 1-D standard Earth model AK135 (Kennett et al., 1995). The calculation window for a given phase (SK(K)S) is automatically estimated in a time window with 30 seconds length starting five seconds before the theoretical arrival. The selection of the calculation window is performed by considering the signal-to-noise ratio (SNR) of the selected phase relative to both the background noise (before first arrival) and a 20-second window before the selected window (pre-phase SNR). For a phase to be chosen for the subsequent analysis, the background noise SNR and pre-phase SNR are set to be greater than 3.5 and 1.8, respectively. Furthermore, in order to prevent the entry of unwanted P-wave energy into the calculation window of the radial component, the traces with significant energy on the z component in the time window of the selected phase are discarded. Eventually, according to the SNR terms and Z component energy consideration, 1920 waveforms remained.

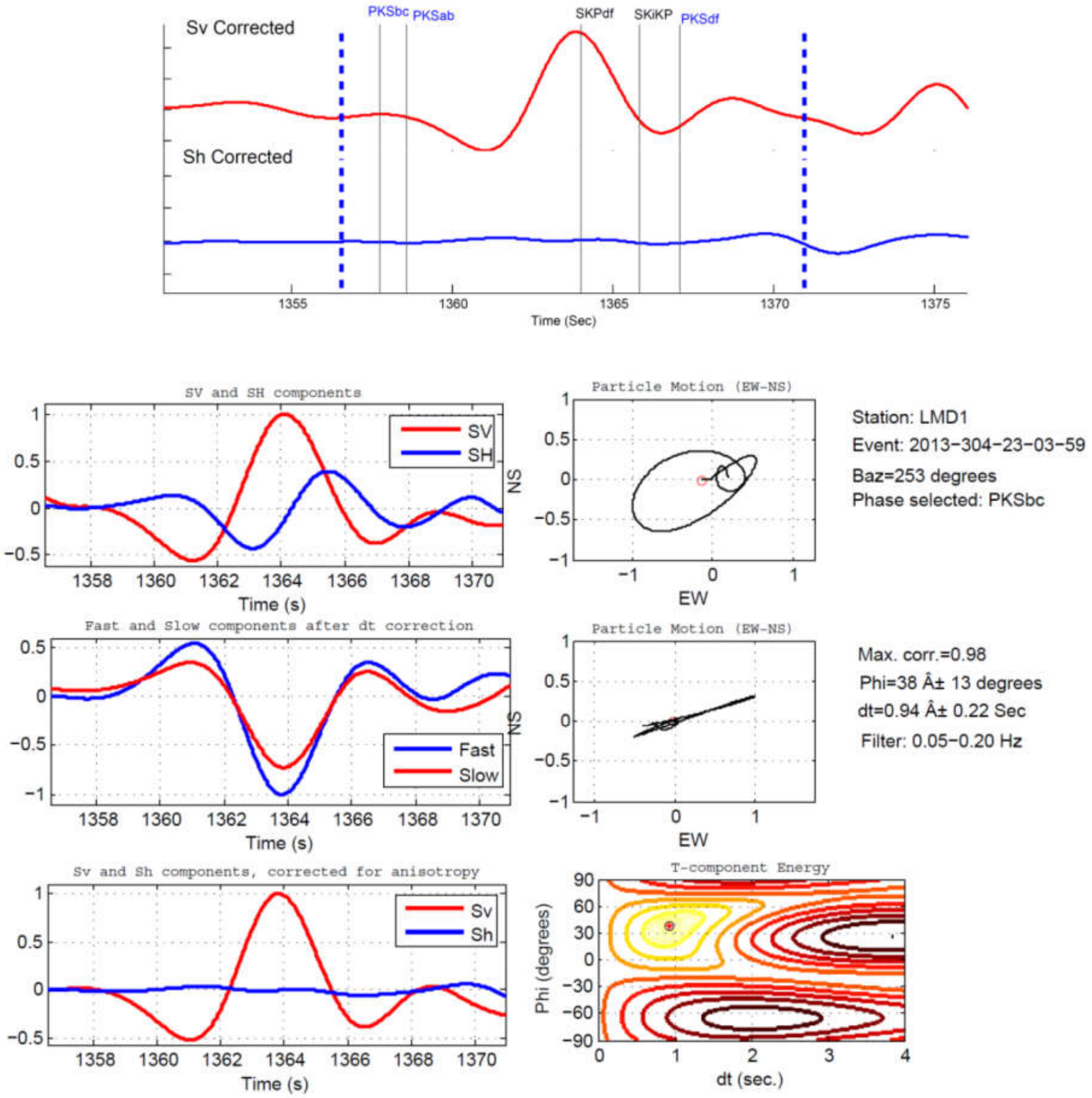

Figure 1. Example of good shear wave splitting measurement on a PKS phase using the method of Silver and Chan (1991). Data are from station LMD1 for an event (Mw 6.6) on October, 31, 2013 located in the South Pacific Ocean at a back azimuth of 253 . Data have been filtered to retain periods between 8 and 25 s.

After the selection of a calculation window for a given phase (SKS, SKKS or PKS), the horizontal traces are rotated into fast and slow directions and time shifts are applied to minimize the energy on the transverse component. For example, one of the results (Figure 1) for the LMD1 station is shown. The above process is also carried out for all the other stations. Finally, after calculation of the anisotropy parameters for each station, only the splitting results with good and fair quality are used.

The quality of splitting measurement (good, fair or poor) is assessed according to the following criteria following Kaviani et al. (2013): (I) the ratio of the mean energy on horizontal components to that of background noise (signal-to-noise, SNR ratio, at least 2), (II) the ratio of the mean energy on the corrected radial and transverse components (should be > 6), (III) the maximum value of cross correlation between the fast and slow components (should be >0.90), (IV) the linearity of the particle motion of the corrected horizontal components, measured by aspect ratio of the particle motion diagram, and (V) the error bars of the estimated splitting parameters (<0.3 s for δt and <30° for Φ).

When the bulk anisotropy beneath a station is too weak to generate any splitting or when the initial polarization of the shear wave is either parallel or perpendicular to the fast direction of the anisotropic medium, the measurements are recognized as "null" with negligible energy on the transverse component (Silver, 1996; Savage, 1999; Long and Silver, 2009). This is identified by the observation of weak energy on the uncorrected transverse component and a nearly linear initial particle motion (Silver and Chan, 1991).

Then, the individual splitting measurements at each station are used to calculate average splitting parameters assuming a one-layer anisotropy. For this purpose, a mean value of split delay times is used (each station should have at least five measurements) as the delay time of the equivalent one-layer model. The fast axis of the one-layer model is

Table 2. The anisotropy results obtained from the one-layer modeling for all stations in the study area.

Station	Stat_lat (°)	Stat_lon (°)	Filter (S)	Phi (°)	Dt (S)	num_obs	Phi_rms (°)	dt_rms (S)	total_rms
MAHB	36.77	45.71	5—20	132	1.5	24	30.4	0.56	1.54899
DHR	34.7	46.39	5—20	166	1	23	41.7	0.47	1.48264
LIN	34.92	46.96	5—20	6	1	8	43.7	0.29	1.52625
BZA	34.47	47.86	5—20	52	1.4	31	34	0.54	1.74574
KOM	34.18	47.51	5—20	32	1.2	37	41.6	0.64	1.79828
KCHF	34.27	47.04	5—20	142	1.3	14	25.5	0.54	1.31798
KFM	33.52	47.85	5—20	58	1.2	12	37.5	0.49	1.8345
KMR	33.52	48.38	5—20	68	1.1	16	16.7	0.43	1.87521
HAGD	34.82	49.14	5—20	31	1.6	14	37.2	0.49	1.56775
HKZM	35.38	48.9	5—20	118	1.2	7	25.8	0.32	1.71889
HSAM	34.21	48.6	5—20	53	1.3	37	34.1	0.51	1.9055
KLNJ	31.01	51.59	5—20	151	1.4	46	36	0.49	1.3098
AHWZ	31.33	48.64	5—20	48	1.4	15	19.2	0.61	1.8673
AMIS	31.67	49.29	5—20	151	1.2	9	40.4	0.46	1.39482
ABH1	30.6	50.25	5—20	11	1.5	8	32.7	0.45	1.13379
SHK1	32.33	50.88	5—20	26	1.6	9	40.8	0.65	1.43586
SHI	29.64	52.52	5—20	132	1.3	36	44.8	0.52	1.73376
LMD1	27.34	53.16	5—20	28	1.2	48	19.7	0.49	1.81601
LAR1	27.67	54.37	5—20	54	1.6	6	8.2	0.46	1.51072
JHRM	28.5	53.58	5—20	54	1.1	24	32	0.52	1.66042
DHL1	32.68	47.28	5—20	20	1.1	6	30.6	0.39	0.9873
BNB	27.45	56.54	5—20	154	1.2	24	27.4	0.57	1.20199
GENO	27.4	56.17	5—20	10	1	59	37.2	0.48	1.30022
JSK1	25.64	57.77	5—20	50	1.3	5	27.6	0.47	1.6001
KHNJ	27.95	57.71	5—20	26	1.4	15	29.9	0.49	1.2733
ROKH	32.4	51.07	5—20	38	1.1	14	43.5	0.5	1.61698
JHBN	32.23	50.67	5—20	61	1.4	8	38.2	0.56	1.52064

taken as an angle that gives minimum stacked angular difference with all individual fast axes for the given station. The results of this one-layer modeling are shown in Table 2. The values of splitting parameters of the one-layer model beneath each station and corresponding misfit errors of the delay times and fast axes as well as weighted value of the combined misfit error are also given in Table 2.

An example of this one-layer modeling is shown in Figure 2 for LMD1 station. A map of all individual splitting measurements (red bars) as well as the parameters of the equivalent one-layer models (blue bars) are shown in Figure 3.

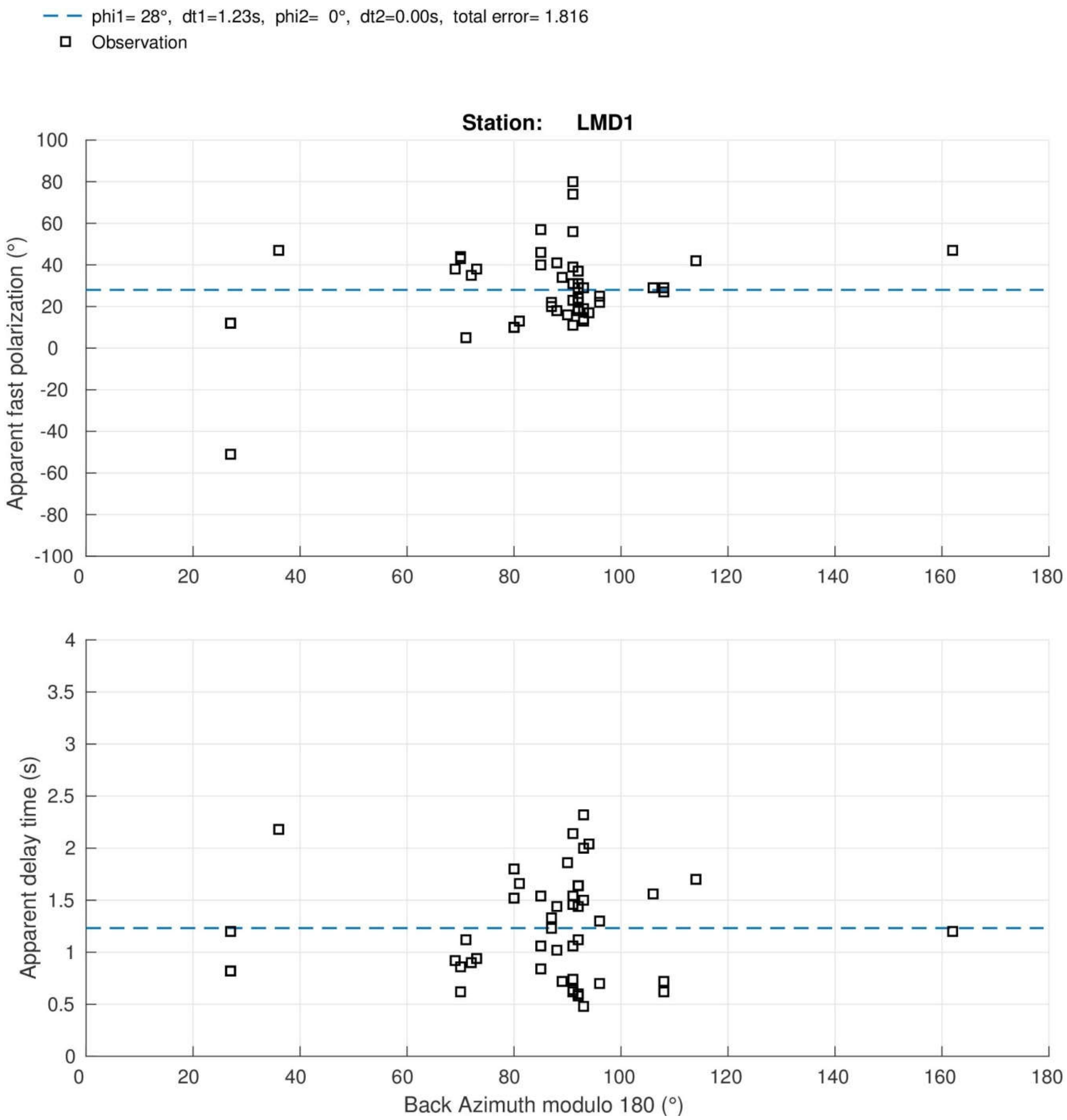

Figure 2. Results for LMD1 station were modeled with method of Silver and Savage (1994), considering the ground with one layer anisotropy. The top figure represents the value obtained for φ parameter (blue dashed line) and the lower figure represents (blue dashed line) the δt parameter.

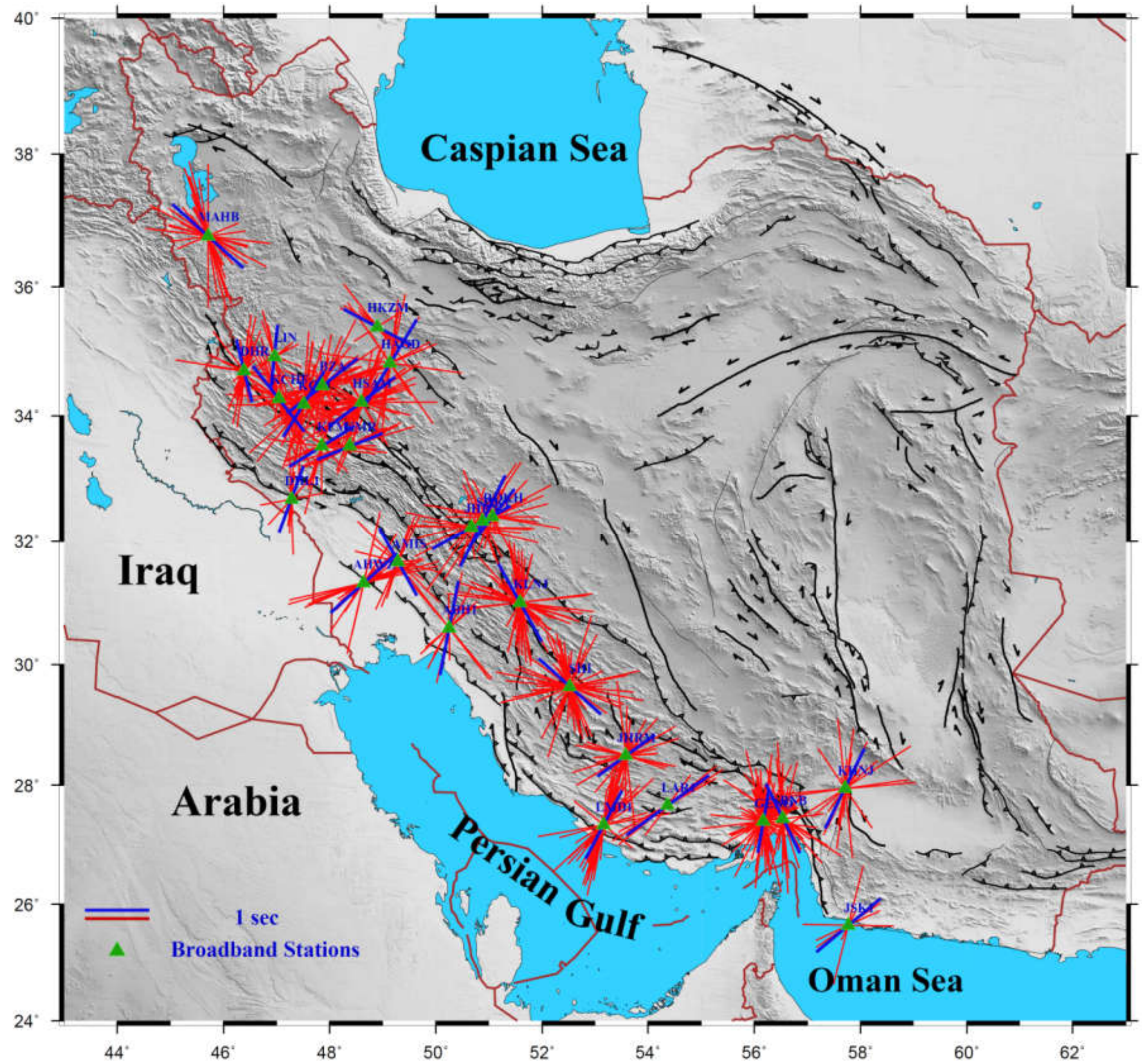

Figure 3. Anisotropy results**.** Red bars indicate results obtained for strength and trend of seismic anisotropy beneath the Zagros stations. Blue bars indicate modeling results based on the method of Silver and Savage (1994), for the ground with the assumption of one layer anisotropy.

4 Discussion and conclusions

The average one-layer model of anisotropy exhibits a relatively complex pattern beneath the Zagros (Figure 3). Though the majority of stations show fast axes in the NE-SW (normal to the trend of the mountain range) direction, yet at some stations, an NW-SE directions (parallel to the trend of the mountain range) is observed. The splitting delay time (δt) is calculated in the range of 0.5 to 1.5 seconds. Kaviani et al. (2009) using a limited data set reported mainly null splitting observations in the Zagros. However, Keshvari et al. (2011), using variations in the relative S-residuals, observed an apparent effect resulting from anisotropy beneath the profile that crosses the Zagros belt. Our long-term observation also reveals that the anisotropy beneath the Zagros is rather complex not null. In compressional tectonic regimes such as the Zagros belt, a pure shear deformation in the mantle that could develop lattice preferred orientation (and anisotropic directions) subparallel to the strike of the belt is expected. As the strain rate map of Raeesi et al. (2017) (Figure 4) also shows, the expected direction of the maximum strain rate is subparallel to the strike of the belt in the Zagros. If the main cause of the observed SKS splitting directions in the Zagros was the anisotropy in the lithosphere, we should have had fast axes subparallel to the strike of the belt, that is mainly in NW-SE direction. However, our findings show that the majority of the fast axes (about 20 stations) are oriented orthogonal to the belt. Therefore, it is argued here that the anisotropy developed due to both the deformation in the lithosphere and flow in the asthenosphere has caused the pattern of the shear-wave splitting observed in Zagros.

If the anisotropy in the asthenosphere is due to the relative motion between the lithospheric plate and the asthenosphere, fast directions subparallel to the Absolute Plate Motion (APM) direction of the lithospheric plates are expected. The APM of the Arabian and Eurasian plates (Figure 4) in a No-Net Rotation reference Frame (Argus et al., 2011) shows an NE trending direction. The general trend of the APM and seismic anisotropy in other regions of the Northern Middle East (Turkey for example, Paul et al., 2014) follows the general trend of the APM. This can generally be true for the Iranian Plateau and Zagros too. However, there is a significant structural feature beneath the Zagros that could disturb the simple flow generated by the relative motion of the lithospheric plates over the

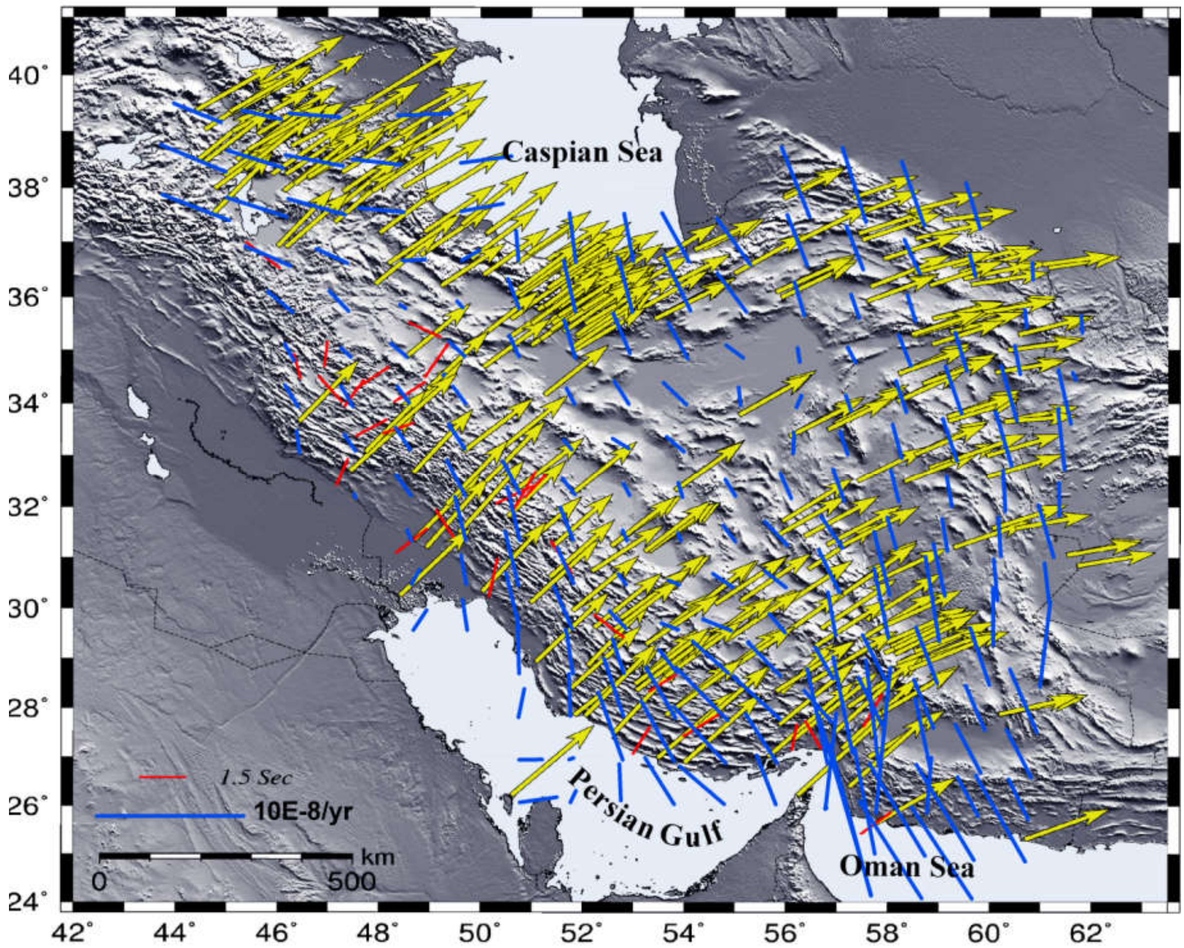

Figure 4. Simultaneous presentation of GPS velocity filed in a No-Net Rotation reference frame (yellow arrows), geodetic shear strain rate map in Iran (blue bars), and this study seismic anisotropy results (red bars) beneath the Zagros collision zone (GPS data from (Argus et al., 2011) and geodetic strain rates are from (Raeesi et al., 2017)).

asthenosphere. Seismic tomography and numerical modeling (Kaviani et al., 2007; Priestley et al., 2012) show that a thick continental keel (root) exists beneath the Zagros. The thickness of the lithosphere is larger than 250 km beneath the Zagros, while it is ~100 km in the adjacent regions. This strong topography of the base of lithosphere and the whole 3-D structure of the keel can cause a 3-D flow around the keel. The same situation has been observed in other regions of the world (e.g. Fouch et al, 2000). This 3-D flow can generate anisotropic fabrics that produce a complex pattern relative to the uniform fabrics generated by the simple flow due to the relative motion of lithosphere over the asthenosphere. On the other hand, the anisotropy in the upper crust should be parallel to the maximum compressional stress direction that is perpendicular to the trend of the Zagros belt in the studied area. Due to the observation of complex anisotropy in this study and according to the resent works on a station in Zagros (Latifi et al, 2018), the contribution of the earth's crust in the calculated anisotropy could not be ignored. Therefore, in order to better understand the anisotropy of the mantle, the Ps splitting analysis of receiver functions are needed to identify the contribution of the crust through the mantle. However, it seems that the main source of the anisotropy is residing in the mantle. In this case, any crustal contribution should be superposed over the mantle contribution. As a general concluding remark, it should be mentioned that, unlike the neighboring regions such as the Anatolian Platea, the pattern of shear-wave splitting across the Zagros and Iranian Plateau implies that there are multiple sources of anisotropy at different depths with lateral variations in strength and direction. The variation of lithospheric thickness is also a dominating factor that makes the pattern of anisotropy more complex. Further numerical modeling aimed at simulating the pattern of anisotropy in case of diverse mode of deformation is required to better explain the observed shear-wave splitting across the Zagros and Iranian Plateau.

Acknowledgments

The authors would like to thank the Iranian Seismological Center (IRSC) affiliated to Institute of Geophysics University of Tehran (IGUT) for providing required waveforms of this study. The figures were generated by the Generic Mapping Tool (GMT) code developed by Wessel and Smith (1998).

References

Alavi, M., 1994, Tectonics of the Zagros orogenic belt of Iran: new data and interpretations, **229**, 211-238.

Argus, D. F., Gordon, R. G. and DeMets, C., 2011, Geologically current motion of 56 plates relative to the no net rotation reference frame: Geochemistry, Geophysics, Geosystems, **12**(11).

Barazangi, M., Sandvol, E., and Seber, D., 2006, Structure and tectonic evolution of the Anatolian plateau in eastern Turkey: Geological Society of America, special papers, **409**, 463–473.

Berberian, M., 1995, Natural Hazards and the First Earthquake Catalogue of Iran, Volume 1: Historical Hazards in Iran Prior to 1900. A UNESCO/IIEES Publication during UN/IDNDR, 649 p., IIEES, Tehran.

Dewey, J., Hempton, M., Kidd, W., Saroglu, F. T., and Şengör, A., 1986, Shortening of continental lithosphere: the neotectonics of Eastern Anatolia—a young collision zone, **19**, 1-36.

Fouch, M. J., Fischer, K. M., Parmentier, E. M., Wysession, M. E., and Clarke, T. J., 2000, Shear wave splitting, continental keels, and patterns of mantle flow: Journal of Geophysical Research, Solid Earth, **105**(B3), 6255-6275.

Jackson, J., and McKenzie, D., 1984, Active tectonics of the Alpine–Himalayan Belt between western Turkey and Pakistan: Geophysical Journal International, **77**(1), 185-264.

Jung, H., and Karato, S. I., 2001, Water-induced fabric transitions in olivine: Science, **293**(5534), 1460-1463.

Jung, H., Mo, W., and Green, H. W., 2009, Upper mantle seismic anisotropy resulting from pressure-induced slip transition in olivine: Nature Geoscience, **2**(1), 73.

Karato, S.I., Jung, H., Katayama, I. and Skemer, P., 2008. Geodynamic significance of seismic anisotropy of the upper mantle: new insights from laboratory studies. Annu. Rev. Earth Planet. Sci., 36, 59-95.

Karato, S. I., 2012, Deformation of earth materials: an introduction to the rheology of solid earth: Cambridge University Press.

Kaviani, A., Paul, A., Bourova, E., Hatzfeld, D., Pedersen, H., and Mokhtari, M., 2007, A strong seismic velocity contrast in the shallow mantle across the Zagros collision zone (Iran): Geophysical Journal International, **171**(1), 399-410.

Kaviani, A., Hatzfeld, D., Paul, A., Tatar, M., and Priestley, K., 2009, Shear-wave splitting, lithospheric anisotropy, and mantle deformation beneath the Arabia–Eurasia collision zone in Iran: Earth and Planetary Science Letters, **286**(3), 371-378.

Kaviani, A., Hofstetter, R., Rümpker, G., and Weber, M., 2013, Investigation of seismic anisotropy beneath the Dead Sea fault using dense networks of broadband stations: Journal of Geophysical Research, Solid Earth, **118**(7), 3476-3491.

Kennett, B. L. N., Engdahl, E. R., and Buland, R., 1995, Constraints on seismic velocities in the earth from travel times: Geophysical Journal International, **122**, 108-124.

Kearey, P., Brooks, M., and Hill, I., 2013, An introduction to geophysical exploration: John Wiley and Sons.

Keshvari, F., Shomali, Z. H., Tatar, M., and Kaviani, A., 2011, Upper-mantle S-velocity structure across the Zagros collision zone resolved by nonlinear teleseismic tomography: Journal of Seismology, **15**(2), 329-339.

Latifi, K., Kaviani, A., Rümpker, G., Mahmoodabadi, M., Ghassemi, M. R., and Sadidkhouy, A., 2018, The effect of crustal anisotropy on SKS splitting analysis—synthetic models and real-data observations: Geophysical Journal International, **213**(2), 1426-1447.

Long, M. D., and Silver, P. G., 2009, Shear wave splitting and mantle anisotropy: measurements, interpretations, and new directions: Surveys in Geophysics, **30**(4-5), 407-461.

Mainprice, D., 2007, Seismic anisotropy of the deep Earth from a mineral and rock physics perspective. In: Schubert G (ed) Treatise on geophysics, Elsevier, Oxford, **2**, 437–49.

Paul, A., Karabulut, H., Mutlu, A. K., and Salaün, G., 2014, A comprehensive and densely sampled map of shear-wave azimuthal anisotropy in the Aegean–Anatolia region: Earth and Planetary Science Letters, **389**, 14-22.

Priestley, K., McKenzie, D., Barron, J., Tatar, M., and Debayle, E., 2012, The Zagros core: deformation of the continental lithospheric mantle: Geochemistry, Geophysics, Geosystems, **13**(11).

Raeesi, M., Zarifi, Z., Nilfouroushan, F., Boroujeni, S. A., and Tiampo, K., 2017, Quantitative Analysis of Seismicity in Iran: Pure and Applied Geophysics, **174**(3), 793-833.

Savage, M. K., 1999, Seismic anisotropy and mantle deformation: what have we learned from shear wave splitting?: Reviews of Geophysics, **37**(1), 65-106.

Sella, G. F., Dixon, T. H., and Mao, A., 2002, REVEL, A model for recent plate velocities from space geodesy, Journal of Geophysical Research, Solid Earth, **107**(B4).

Sepehr, M., and Cosgrove, J. W., 2005, Role of the Kazerun Fault Zone in the formation and deformation of the Zagros Fold Thrust Belt, Iran: Tectonics, **24**(5).

Sileny, J., and Plomerova, J., 1996, Inversion of shear-wave splitting parameters to retrieve three-dimensionalorientation of anisotropy in continental lithosphere: Physics of the Earth and Planetary Interiors, **95**, 277–292.

Silver, P. G., and Chan, W. W., 1991, Shear wave splitting and subcontinental mantle deformation: Journal of Geophysical Research, Solid Earth, **96**(B10), 16429-16454.

Silver, P. G., and Savage, M. K., 1994, The interpretation of shear-wave splitting parameters in the presence of two anisotropic layers: Geophysical Journal International, **119** (3), 949–963.

Silver, P. G., 1996. Seismic anisotropy beneath the continents, Probing the depths of geology: Annual Review of Earth and Planetary Sciences, **24**(1), 385-432.

Sleep, N. H., 1997, Lateral flow and ponding of starting plume material: Journal of Geophysical Research, Solid Earth, **102**(B5), 10001-10012.

Sleep, N. H., Ebinger, C. J., and Kendall, J. M., 2002, Deflection of mantle plume material by cratonic keels: Geological Society, London, Special Publications, **199**(1), 135-150.

Snyder, D. B., and Barazangi, M., 1986, Deep crustal structure and flexure of the Arabian plate beneath the Zagros collisional mountain belt as inferred from gravity observation: Tectonics, **5**(3), 361-373.

Stein, S., and Wysession, M., 2009, An introduction to seismology, earthquakes, and earth structure: John Wiley and Sons.

Vecsey, L., Plomerova, J., and Babuska, V., 2008, Shear-wave splitting measurements—problems and solutions: Tectonophysics, **462**, 178–196.

Vinnik, L. P., Makeyeva, L. I., Milev, A., and Usenko, A. Y., 1992, Global patterns of azimuthal anisotropy and deformations in the continental mantle: Geophysical Journal International, **111**(3), 433-447.

Vinnik, L. P., Farra, V., and Romanowicz, B., 1989, Azimuthal anisotropy in the Earth from observations of SKS at Geoscope and NARS broadband stations: Bulletin of the Seismological Society of America, **79**(5), 1542-1558.

Waltham, T., 2014, Foundations of engineering geology: CRC Press.

Wessel, P., and Smith, W. H., 1998, New, improved version of Generic Mapping Tools released: Eos, Transactions American Geophysical Union, **79**(47), 579-579.